Eur. Phys. J. D **39**, 439–444 (2006)
DOI: 10.1140/epjd/e2006-00126-y

THE EUROPEAN PHYSICAL JOURNAL D

Possibility of plasma density diagnostics using Langmuir-wave-caused dips observed in dense laser plasmas

F.S. Krasniqi[1,a], O. Renner[1,2], E. Dalimier[3], E. Dufour[3], R. Schott[3], and E. Förster[1]

[1] Institut für Optik und Quantenelektronik, Friedrich-Schiller-Universität, Max-Wien-Platz 1, 07743 Jena, Germany
[2] Institute of Physics, Academy of Sciences CR, Na Slovance 2, 18221 Prague, Czech Republic
[3] Physique Atomique dans les Plasmas Denses, Laboratoire pour l'Utilisation des Lasers Intenses, CNRS-École Polytechnique-CEA-Université Paris VI, 75252 Paris Cedex 05 and 91128 Palaiseau Cedex, France

Received 2 November 2005 / Received in final form 20 March 2006
Published online 13 June 2006 –

Abstract. A systematic study of the Langmuir-wave-caused dips (L dips) observed in profiles of the Al Ly γ line emitted from laser irradiated sandwich targets indicates that these fine spectral features can be used as a tool for density diagnostics in intermediately coupled plasmas. The spectroscopic data required for a reliable identification of L dips were collected by a vertical-geometry Johann spectrometer providing high spectral and spatial resolution. The electron densities deduced from the evolution of the L dips along the laser target axis compare well with those derived from hydrosimulations and from measurements of the line widths and shifts.

PACS. 32.70.Jz Line shapes, widths, and shifts – 52.70.La X-ray and gamma-ray measurements

1 Introduction

Space resolved X-ray spectroscopy of multicharged ions has proven to be a powerful diagnosis technique for the study of dense plasmas. The spectral lines emitted from such plasmas are capable of providing information particularly on electron density, electron temperature and ionization stage [1–3]. The spectroscopic measurements of the plasma density are typically based on widths of the emitted line profiles; the spectra are most frequently analyzed by consideration of the Stark broadening due to electrons and ions. In addition to quasistatic particle-produced fields, radiating ions are subjected to a simultaneous action of high frequency electric field originating from electronic plasma oscillations (Langmuir oscillations). The interaction of the radiators with both these fields leads to an appearance of fine structure within the spectral line profile which can be observed as satellites at shoulders of the emitted spectral lines [4] or as local depressions (hereafter L dips) at definite separations $\Delta\lambda$ from the line center [5,6]. General considerations concerning the visibility of these phenomena are subject of a paper [7]. The detailed theory [8] suggests that L dips result from the resonance coupling of Langmuir oscillations electric field with ion microfield. Their location from the line center depends on the electron density and their width depends on amplitude of the dynamic electric field. Thus assuming that L dips are sufficiently resolved, they can provide an independent method for determining the electron density N_e of the emitting plasma region and for measuring the amplitude of the quasimonochromatic electric field E_0. L dips were discovered experimentally in profiles of hydrogen spectral lines [9] and explained theoretically in papers [9–12]. The existence of these dips was confirmed in later experiments at linear-, θ-, and z-pinches (see, e.g., [6,8] and references therein). Successful observation of L dips in laser produced plasmas is connected with the development of novel X-ray spectrometers combining high spectral and spatial resolution. The first experimental evidence for their occurrence in hot and dense Al plasmas is reported in [13].

In the present article we report on the use of L dips to diagnose the laser produced plasmas. Benefiting from an ultrahigh resolution spectrometer and specially designed targets we reliably identified L dips in spectral profiles of the Lyman series Al Ly γ line and used them to infer the electron density of the emitting plasma as a function of a distance from the laser-irradiated target surface. The data are compared with those derived by means of line widths, line shifts and 1D hydrodynamic simulations.

[a] *Present address*: Paul Scherrer Institute, Swiss Light Source, 5232 Villigen PSI, Switzerland.
e-mail: faton.krasniqi@psi.ch

2 Theoretical approach

An analytical theory of the L dip phenomenon was presented in [6,8]. In this section we briefly survey conclusions relevant to our experiment.

The central point of the L dip phenomenon is a resonant coupling between a quasistatic electric field **F** (usually represented by the low-frequency part of the ion microfield in plasmas) and the quasimonochromatic electric field of the Langmuir oscillations $\mathbf{E} = \mathbf{E}_0 \cos(\omega_p t + \phi)$. Here $\omega_p = (4\pi e^2 N_e/m)^{1/2}$ is the plasma frequency, e and m are the electron charge magnitude and electron mass. In the dipole approximation (first order perturbation), the level of a radiator with the principal quantum number n splits under the action of the electric field **F** into $(2n-1)$ equidistant Stark sublevels. In high density plasmas the spatial non-uniformity becomes essential and the first-order perturbation is not valid. This means that a dipole approximation is no longer sufficient for describing the interaction of a radiator with perturbing ions and higher multi-poles (at least quadrupole term) have to be taken into account. When the quadrupole interaction of the radiator with the perturbing ions is taken into account, a separation $\Delta\omega_{q+}$ between Stark sublevels with electric quantum numbers q and $q+1$ differs from a separation $\Delta\omega_{q-}$ between Stark sublevels q and $q-1$ ($q = n_1 - n_2$, n_1 and n_2 being the parabolic quantum numbers). The resonant coupling between a quasistatic electric field **F** and a quasimonochromatic electric field **E** is reached when the separation between two neighboring Stark sublevels, $\Delta\omega_q$, is equal to a multiple of plasma frequency ω_p, i.e., $\Delta\omega_q = k\omega_p$, where k is the number of the quanta involved in the resonance. In the case of the first order resonance $k = 1$.

In the profiles of the Lyman lines ($np \rightarrow 1s$), the first order resonance manifests as two L dips (L^+ and L^- dips) whose position from the line center, $\Delta\lambda_{q\pm}$, is

$$\Delta\lambda_{q\pm} \approx -\frac{\lambda_0^2}{2\pi c}\left(q\omega_p + C_{q\pm}\sqrt{\frac{2}{27n^3 Z_p Z_r}\frac{\omega_p^3}{\omega_a}}\right) \quad (1a)$$

$$C_{q\pm} = n^2(n^2 - 6q^2 - 1) + 6n^2 q(2q \pm 1) \quad (1b)$$

where Z_r is the nuclear charge of the radiator, Z_p is the charge of the perturbing ions, $\omega_a = me^4\hbar^{-3} \approx 4.14 \times 10^{16}$ s^{-1} is the atomic unit of frequency, and λ_0 is the unperturbed wavelength. The first term in equation (1a) reflects the dipole interaction with the ion microfield; the second term takes into account — via the quadrupole interaction — a spatial nonuniformity of the ion microfield. For $q = 0$ the first term vanishes and there is only one dip, the central dip.

Each L dip represents a structure consisting of the dip itself (the intensity minimum at the location given by Eq. (1)) and two surrounding bumps [6,8]. The bumps are due to the fact that the mechanism of the dip formation consists of a partial transfer of the intensity from the wavelength of the dip to adjacent wavelengths on each side of the dip. In the profiles of the Al Ly γ line emitted from intermediately coupled plasmas, typically five L dips might be observed close to the unperturbed wavelength λ_0. These five dips correspond to $q = -1$ (red dips L^+ and L^-), $q = 0$ (the central L dip), and $q = 1$ (blue dips L^+ and L^-). The density dependence of the calculated positions of the red L dips, which are well visible in emission of the Al Ly γ investigated in our experiment, is shown in Figure 1. The blue L dips are generally positioned too far in the blue wing, i.e., in the noisy signal, and the central dip is near the unperturbed wavelength and the intensity maximum, so that it is not clearly visible.

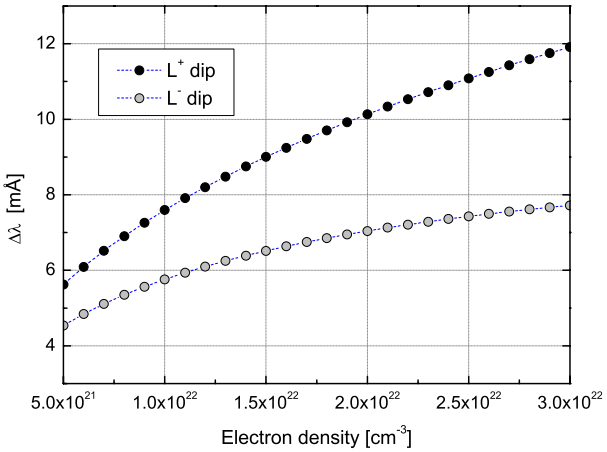

Fig. 1. Density dependence of the calculated positions of the most important L dips in the Al Ly γ line profile observed in our experiments. The L dips (L^- and L^+) correspond to Stark sublevel $q = -1$.

3 Experimental set-up

The experiment was carried out on the nanosecond laser facility at the LULI École Polytechnique, Palaiseau, France [13]. The scheme of the experimental geometry is shown in Figure 2. A single laser beam delivering up to 10 J of the frequency-quadrupled radiation (0.263 μm) in a pulse length of 0.5 ns was focused to a spot with a diameter of 80–100 μm, yielding intensity of the order of $1\text{–}2 \times 10^{14}$ W/cm^2. The radiation was incident onto a structured target consisting of a 50 μm-thick aluminum foil sandwiched between two CH substrates (each 25 μm thick, hereafter Al/CH target) or alternatively between two Mg substrates (each 10 μm thick, hereafter Al/Mg target).

By placing the sandwiched target through the center of the focal spot, the transverse plasma gradients were suppressed, the aluminum ions were kept in a constrained flow perpendicular to the direction of the spectra observation and the effective plasma parameters were optimized to the values favorable for the dip observation (hydrodynamic simulations estimate the electron density and temperature close to the irradiated target surface at about 3×10^{22} cm^{-3} and 300 eV, respectively). The spectra were recorded in single laser shots and observed at an angle of $\psi = 2.0° \pm 0.7°$ to the irradiated target surface.

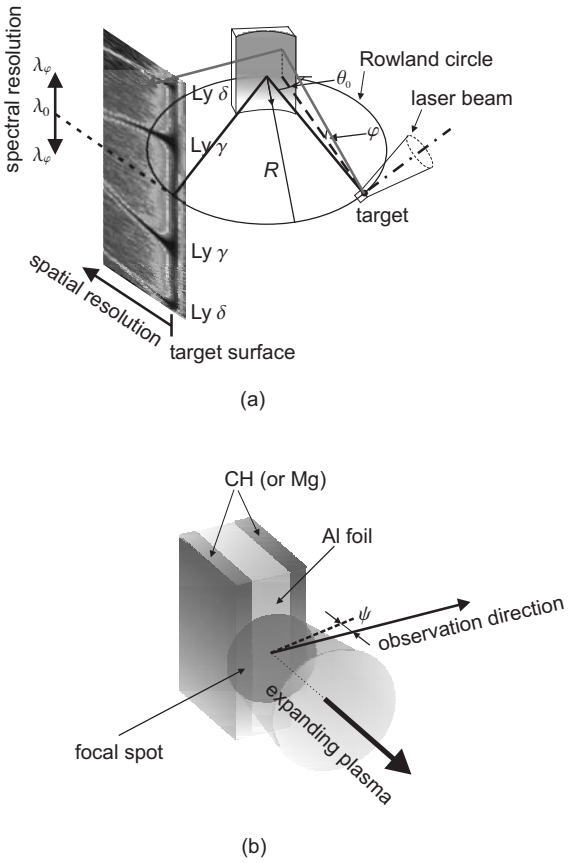

Fig. 2. The spectrometer (a) and the geometry of the target (b). The wavelengths λ_φ of the diffracted radiation are dispersed as a function of the vertical divergence angle φ, ψ is the angle of the spectra observation with respect to the target surface. The expansion of Al ions is spatially constrained by a plasma created at CH or Mg substrates.

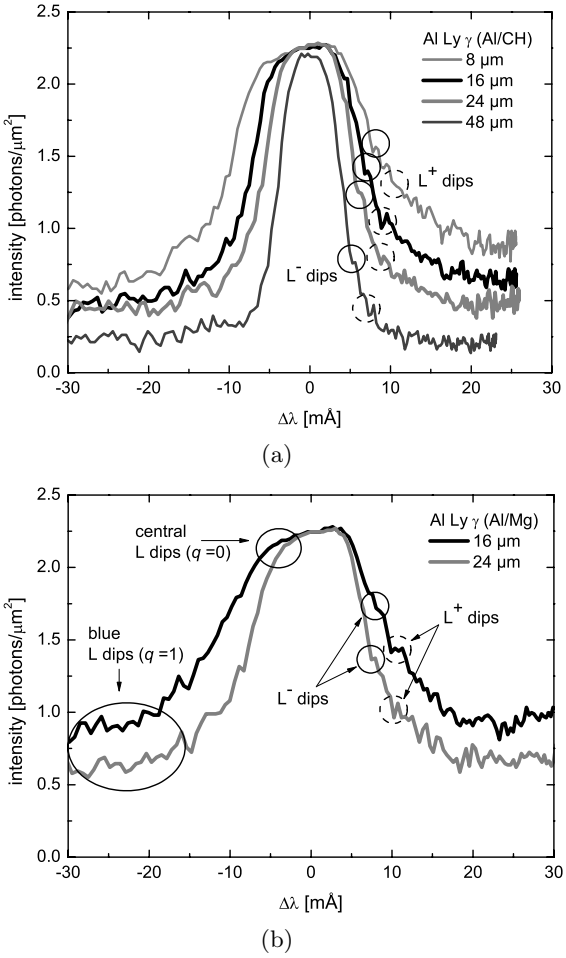

Fig. 3. Al Ly γ emission measured at the distances 8–48 μm from the surface of laser irradiated (a) Al/CH and (b) Al/Mg target. The red L^- and L^+ ($q = -1$) dips used for density diagnostics are marked with solid and dashed circles, respectively. The regions with the anticipated occurrence of the central and blue L dips are marked with ellipses in (b).

The high-dispersion spectroscopic data required for identification of fine spectral features in the line profiles were collected by a vertical-geometry Johann spectrometer (VJS) [14]. The instrument disperses the radiation in a direction parallel to the axis of the cylindrically bent crystal, i.e., as a function of the vertical divergence angle φ (see Fig. 2), and thus records two identical sets of spatially resolved spectra symmetrically located with respect to the maximum central wavelength λ_0 (corresponding to the Bragg angle θ_0). The simultaneous production of a pair of symmetric spectra provides a reference point for the computational reconstruction of the spectroscopic data and, at the same time, considerably increases the experimenter's confidence in reproducibility of relatively tiny details in profiles of the emitted spectral lines. As discussed below, this point was crucial for reliable identification of the L dips.

The VJS is equipped with a crystal of quartz (100) cylindrically bent to a radius of 77.2 mm. The source and the detector are positioned on the Rowland circle and the spectra are recorded with 1D spatial resolution of few micrometers (obtained in a direction perpendicular to that of dispersion, see Fig. 2a). The ray tracing calculations suggest that for the Al Ly γ, the VJS provides spectral resolution of 4200 and average linear dispersion of 175 mm/Å. For sources extended along the normal to the target surface, the Bragg angle of the central ray θ_0 decreases with increasing distance of the emitting region from the Rowland circle. This explains the arched character of the spectral lines recorded at the detector, as shown in insertion of Figure 2a.

The spectra were recorded on the X-ray film Kodak Industrex CX, the spatial resolution was limited to 8 μm by the densitometer slit. The spectra were evaluated by using the algorithm described in [14].

4 Experimental results and interpretation

Figures 3a and 3b show the profiles of the Al Ly γ lines emitted from laser irradiated Al/CH and Al/Mg targets, respectively. The profiles display several tiny features which are well reproducible in symmetric spectra

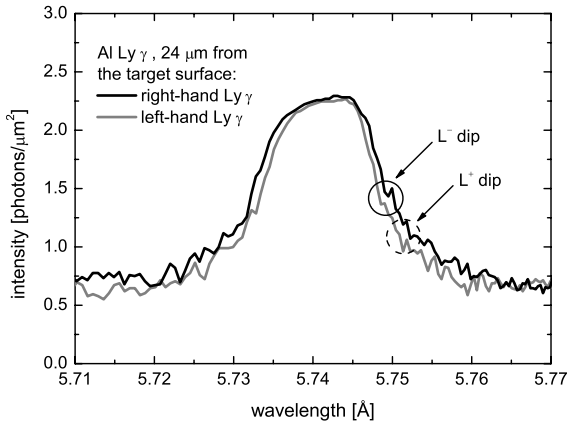

Fig. 4. The left- and right-hand sides of the Al Ly γ spectrum emitted at the distance of 24 μm from the laser-irradiated Al/Mg target surface; L-dip-bump structures are marked with circles.

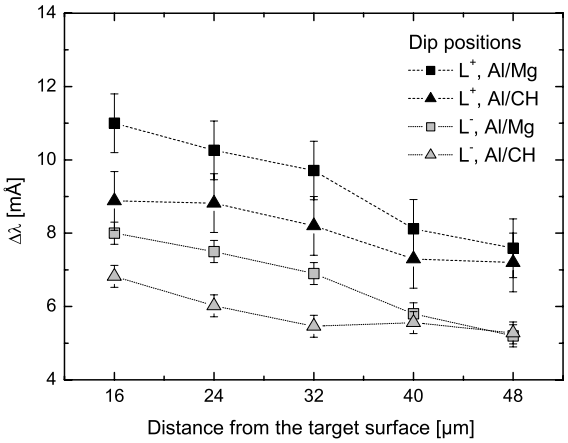

Fig. 5. The measured space-dependent positions $\Delta\lambda$ of the L^- and L^+ dips from the line center.

and move systematically with the decreasing distance from the target surface, i.e., with the increasing electron density. Albeit the intensity modulations observed close to the center and at the blue side of the spectral lines also indicate some degree of reproducibility, we have restricted to a detailed analysis of the most pronounced dips appearing at the red side of the line profiles where the VJS provides extremely large linear dispersion and thus the most reliable data. These features are labelled as L^- and L^+. They represent the red L^- and L^+ dips, see Section 2. For the density diagnostics we use both the red L^- and L^+ dips. Generally, the visibility of L^+ dip is better than that of L^- dip (due to the fact that the coupling between the sublevels $q = -1$ and $q = 0$ is noticeably stronger than the coupling between the sublevels $q = -1$ and $q = -2$ [6]), and its density dependence is stronger than that of the L^- dip; However, since L^+ dips are located further from the line center where the statistical noise is larger, for the density diagnostics, larger uncertainties are associated. Our confidence in a correct identification of the L dips is mainly based on the outstanding property of VJS to produce simultaneously two mirror spectra (as mentioned in Sect. 3); in other words, any real feature observed in one side of the spectra should also be observed in the symmetric part. As shown in Figure 4 where the left- and right-hand spectra of the Al Ly γ are compared, the fine structures observed in both mirror-symmetric spectral records are nearly identical. The comparison of these profiles indicates a degree of confidence in reliable identification of fine spectral features; partial discrepancies in both spectra (in particular, different line widths) may be ascribed to a slight misalignment of the densitometered film resulting in a spatial misfit of a ± 4 μm between both records, and to statistical intensity fluctuations on the detector. Additionally, the modulation of the intensity by the most pronounced bump-dip-bump structures approaches 10%, while the standard deviation of the intensity measurement at the locations of these dips is between 3 and 4%. For all laser shots providing comparable irradiation of the targets, the spectra demonstrate similar qualitative features. Our analysis of several Al Ly γ line profiles emitted from different regions close to the target surface identifies these features as L dips. They cannot be attributed to the charge-exchange X dips [15,16]) which occur in heterogeneous plasmas (e.g. AlC plasma) and in contrast to Langmuir dips, their positions are stable when varying the density.

The distance $\Delta\lambda$ of the L^- and L^+ dips from the line center decreases with the decreasing electron density (cf. Fig. 1) but also the intensity and the FWHM of the spectral lines drop rapidly; consequently the L dips begin to merge into noise. The detailed shape and the visibility of the L dips are discussed in papers [7,13]. The lower and upper limits that determine the range of electron densities where the L dips could be reliably identified in our measurements are about 5×10^{21} cm^{-3} and 3×10^{22} cm^{-3}, respectively.

Figure 5 shows that for the laser-irradiated Al/CH target, the position of the L^- (L^+) dip from the line center decreases from approximately 7 mÅ (9 mÅ), as observed at the distance of about 16 μm from the target surface, to 5 mÅ (7 mÅ) at 48 μm, whereas for the Al/Mg target, it decreases from 8 mÅ (11 mÅ) to about 5 mÅ (8 mÅ). Taking into account that the dip position from the line center depends on the electron density of the emitting plasma N_e (via ω_p, see Eq. (1)), this behavior of the L^- and L^+ dips (i) complies with the expected distance-dependent decrease of the plasma density and (ii) indicates that the Mg substrates (as compared with the CH substrates) provide better lateral confinement for the Al plasma. More generally, precise measurements of L dip positions obviously offer an alternative method for the plasma density diagnostics.

To support quantitatively this conjecture, we compare the electron densities deduced from the L dip positions with the hydrodynamic plasma simulations and with alternate methods for the density diagnosis based on the analysis of the spectral line widths and shifts. The plasma evolution was simulated by the 1D hydrodynamic code MEDUSA [17] in a planar geometry. In the version of the

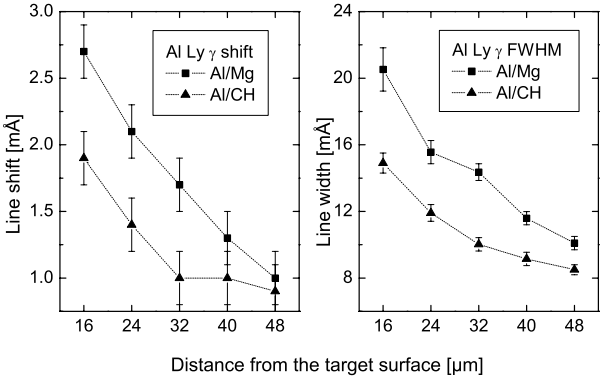

Fig. 6. The space-dependent shifts and widths of the Al Ly γ. The errors of the spectral line widths and positions introduced by fitting the experimental data with pseudo-Voigt profiles amount to about 0.2 mÅ.

code used here, the hydrodynamic equations are supplemented by a time-dependent, non-local thermodynamic equilibrium average-atom model. The effective plasma parameters (electron density and temperature) were averaged over all time steps by using an emission rate of the given spectral line as a weighing factor [18].

The standard methods for the density diagnostics are typically based on precise measurements of the widths and shifts of the emitted spectral lines which both increase with the increasing electron density [19–21]. Here we compare the full experimental profiles of the Al Ly γ with those computed by using the codes IDEFIX [22,23] (for higher densities) and the code PIM PAM POUM [24] (for lower densities). Alternatively, the electron densities are determined from the measured line shifts using the quantum mechanical impact theory [20]. According to this theory, the electron density corresponding to the Lyman line shift $\Delta\lambda$ is

$$N_e[\mathrm{cm}^{-3}] = 1.24 \times 10^{26} \frac{Z_r^2}{(\lambda_0[\text{Å}])^2 D(n,l,T_e)} \Delta\lambda[\text{Å}]$$

where D is the tabulated line shift factor depending on the principal quantum number n, orbital quantum number l, and the electron temperature T_e. The electron temperatures required for determining D are those estimated by means of the MEDUSA.

The shifts and widths of the Al Ly γ measured as a function of the distance above the laser-irradiated target surface are shown in Figure 6. Again, the line shifts and widths increase with the decreasing distance from the target and close to its surface, the Ly γ shift and width observed at Al/Mg target are about 30% and 27%, respectively, larger than those at Al/CH target.

The consistency of hydrodynamic code simulations and experimental methods used for the electron density determination in the range of $N_e > 10^{21}$ cm^{-3} is demonstrated in Figure 7. In the approximation of the 1D code used, the hydrocode calculations predict the same plasma density distribution for both targets, thus it is shown in Figure 7a only. The observed widths and shifts of the spectral lines, as well as the L^- and L^+ dip positions, were related to variations of the electron density along the laser target axis. Obviously, all experimental methods indicate higher plasma densities for Al/Mg than for Al/CH target (in particular, close to the target surface the Al/Mg densities derived by line shifts, L^- (L^+) dips, and line widths are by 30%, 44% (38%), and 72%, respectively, larger). The densities inferred from the L^- dip positions compare favorably with those deduced from the line shifts. In the case of Al/CH target, the results agree to within 8%, whereas for Al/Mg target, the disagreement is less than about 26%. The disagreement with L^+ dip data is slightly larger (up to about 21%), but also the uncertainties in electron densities associated with L^+ dips are larger due to their location near to the noisy signal. The electron densities deduced from hydrodynamic simulations and from the line broadening are generally lower than those inferred from the L dip positions. These discrepancies can be attributed to experimental errors, uncertainties in the line shape fitting procedure, and approximations used in the modelling. The code MEDUSA does not incorporate the possibility to simulate in detail the hydrodynamics of the

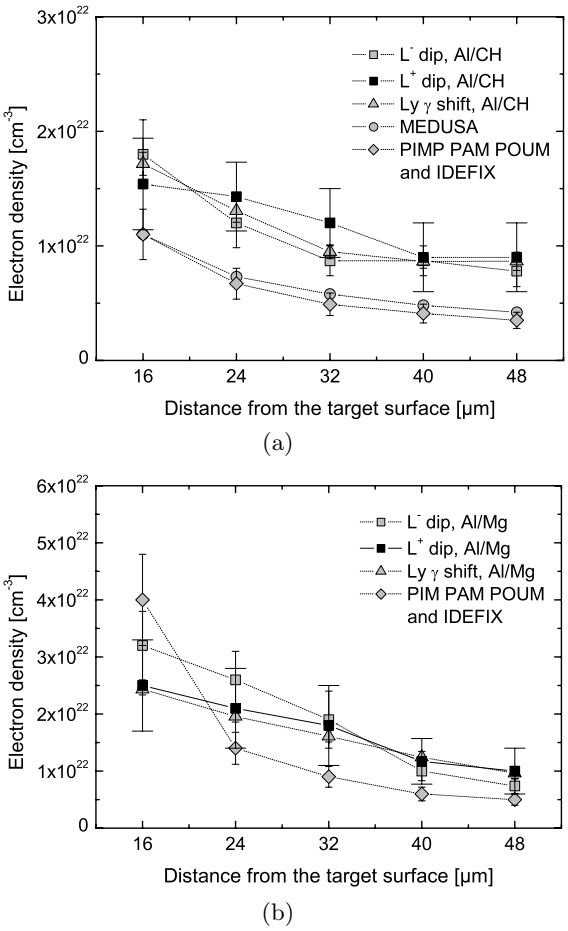

Fig. 7. Comparison of electron densities deduced from Langmuir dips, line shifts, hydrocode MEDUSA, the code IDEFIX (for higher densities) and the code PIM PAM POUM (for lower densities): (a) Al/CH and (b) Al/Mg target. Error bars associated with L^+ dips have larger markers.

structured targets, i.e., it does not distinguish the Al targets sandwiched between Mg or CH substrates. The discrepancies are more pronounced for Al/Mg targets, where the Al plasma confinement is obviously better. However, the results obtained confirm that precisely measured positions of L dips may represent a viable density diagnostics for intermediately coupled plasmas. Alternatively, the L dips may provide a sensitive tool for validation of other diagnostic methods and for testing the theories of radiator-plasma interactions.

5 Conclusions

Benefiting of an advanced X-ray instrumentation and of a sophisticated design of the experimental configuration, we confirmed the presence of reproducible fine structures (dips) in profiles of the spectral line Al Ly γ emitted from the densest part of laser-produced plasmas. We identified the Langmuir-wave-caused dips occurring when the radiating ions interact simultaneously with the ion microfield and the quasimonochromatic electric field originating from the electron plasma oscillations. The electron densities deduced from the positions of the red L dips observed in the Al Ly γ emission of the sandwiched aluminum targets compare well with those derived from the line shifts and the line widths measurements. The results obtained confirm that Mg substrates are superior to CH ones when a higher-degree lateral confinement of Al plasmas is required. The overall agreement among the densities experimentally derived from the Langmuir-wave-caused dips, line widths, shifts, and the 1D plasma modelling suggests that reliably measured positions of the L dips might provide a new efficient tool for plasma diagnostics.

The authors gratefully acknowledge the help of E. Krousky, A. Poquérusse, P. Angelo, P. Sauvan and F. Philippe in performing the experiments, and the assistance of E. Oks in the interpretation of L dip data. This work was partially supported by the BMBF project No. 13N7921 and the DFG project SPP 1134/US17/3. One of the authors (O. Renner) was supported by the Grant Agency of the Czech Republic under Contract No. 202/06/0801.

References

1. V.A Boiko, S.A. Pikuz, A. Ya Faenov, J. Phys. B: At. Mol. Opt. Phys. **12**, 1889 (1979)
2. H.R. Griem, *Spectral Line Broadening by Plasmas* (Academic Press, New York, 1974)
3. D. Chambers, P.A. Pinto, J. Hawreliak, I.R. Al'Miev, A. Gouveia, P. Sondhauss, E. Wolfrum, J.S. Wark, S.H. Glenzer, R. W. Lee, P.E. Young, O. Renner, R.S. Marjoribanks, S. Topping, Phys. Rev. E **66**, 026410-1 (2002)
4. D. Riley, O. Willi, Phys. Rev. Lett. **75**, 4039 (1995)
5. A. Cohn, P. Bakshi, G. Kalman, Phys. Rev. Lett. **29**, 324 (1970)
6. E. Oks, *Plasma Spectroscopy: The Influence of Microwave and Laser Fields* (Springer, New York, 1995)
7. E. Oks, E. Leboucher-Dalimier, Phys. Rev. E **62**, R3067 (2000)
8. E. Oks, St. Böddeker, H.-J. Kunze, Phys. Rev. A **44**, 8338 (1991)
9. A.I. Zhuzhunashvili, E. Oks, Sov. Phys. JETP **46**, 2142 (1977)
10. E. Oks, V.A. Rantsev-Kartinov, Sov. Phys. JETP **52**, 50 (1980)
11. V.P. Gavrilenko, E. Oks, Sov. Phys. JETP **53**, 1122 (1981)
12. V.P. Gavrilenko, E. Oks, Sov. Phys. J. Plasma Phys. **13**, 22 (1987)
13. O. Renner, E. Dalimier, E. Oks, F. Krasniqi, E. Dufour, R. Schott, E. Förster, J. Quant. Spectrosc. Radiat. Transfer **99**, 439 (2006)
14. O. Renner, T. Missalla, P. Sondhauss, E. Krousky, E. Förster, C. Chenais-Popovics, O. Rancu, Rev. Sci. Instr. **68**, 2393 (1997)
15. S. Böddeker, H.-J. Kunze, E. Oks, Phys. Rev. Lett. **75**, 4740 (1995)
16. E. Leboucher-Dalimier, E. Oks, E. Dufour, P. Sauvan, P. Angelo, R. Schott, A. Poquerusse, Phys. Rev. E **64**, 065401 (2001)
17. A. Djaoui, S.J. Rose, J. Phys. B: At. Mol. Opt. Phys. **25**, 2745 (1992)
18. O. Renner, P. Sondhauss, O. Peyrusse, E. Krouský, R. Ramis, K. Eidmann, E. Förster, Laser Part. Beams **17**, 365 (1999)
19. R.W. Lee, J.T. Larsen, J. Quant. Spectrosc. Radiat. Transfer **56**, 535 (1996)
20. H. Nguyen, M. Koenig, D. Berendjem, M. Caby, G. Coulaud, Phys. Rev. A **33**, 1279 (1986)
21. O. Renner, J. Limpouch, E. Krousky, I. Uschmann, E. Förster, J. Quant. Spectrosc. Radiat. Transfer **81**, 385 (2003)
22. P. Gauthier, S.J. Rose, P. Sauvan, P. Angelo, E. Leboucher-Dalimier, A. Calisti, B. Talin, Phys. Rev. E **58**, 942 (1998)
23. P. Sauvan, E. Leboucher-Dalimier, P. Angelo, H. Derfoul, T. Ceccotti, A. Poquerusse, A. Calisti, B. Talin, J. Quant. Spectrosc. Radiat. Transfer **65**, 511 (2000)
24. B. Talin, A. Calisti, L. Godbert, R. Stamm, R.W. Lee, L. Klein, Phys. Rev. A **51**, 1918 (1995)